

Bimetallic RuNi nanoparticles as catalysts for upgrading biomass: metal dilution and solvent effects on selectivity shifts

Miquel Cardona-Farreny,^a Pierre Lecante,^b Jerome Esvan,^c Chiara Dinoi,^d Iker del Rosal,^d Romuald Poteau,^d Karine Philippot,^a M. Rosa Axet^{a*}

^a CNRS, LCC (Laboratoire de Chimie de Coordination), Université de Toulouse, UPS, INPT, 205 route de Narbonne, BP 44099, F-31077 Toulouse Cedex 4, France

^b Centre d'élaboration des matériaux et d'études structurales UPR CNRS 8011, 29 Rue Jeanne-Marvig, BP 4347, 31055 Toulouse, France

^c CIRIMAT, Université de Toulouse, CNRS-INPT-UPS, 4 Allée Emile Monso, BP 44362, 31030 Toulouse, France

^d INSA-CNRS-UPS, LPCNO, Université Fédérale de Toulouse Midi-Pyrénées, 135 Avenue de Rangueil, F-31077 Toulouse, France

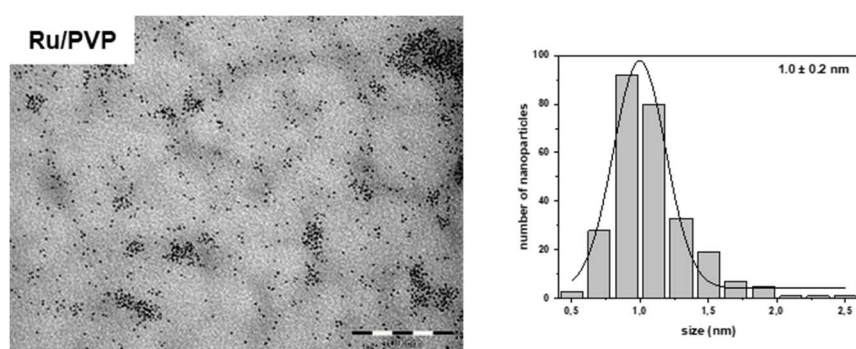


Figure S1. TEM image of Ru/PVP (scale bar 100 nm) together with the respective size histogram.

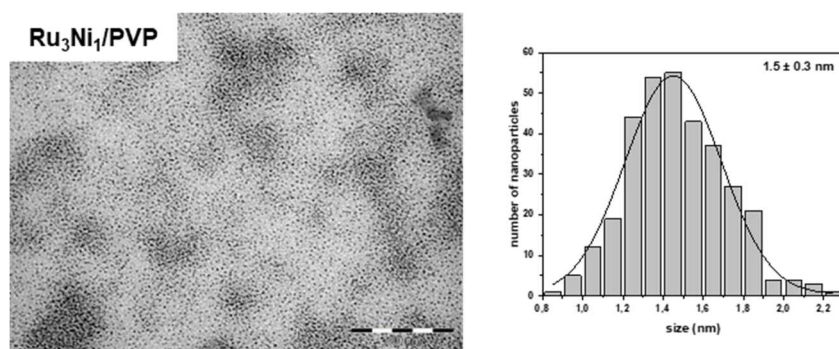


Figure S2. TEM image of Ru₃Ni₁/PVP (scale bar 100 nm) together with the respective size histogram.

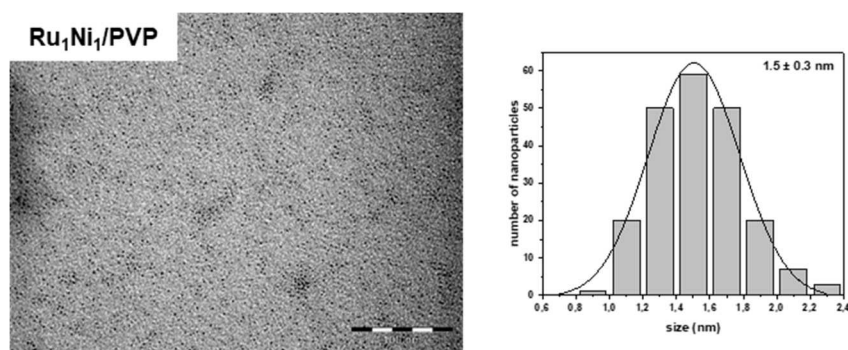


Figure S3. TEM image of Ru₁Ni₁/PVP (scale bar 100 nm) together with the respective size histogram.

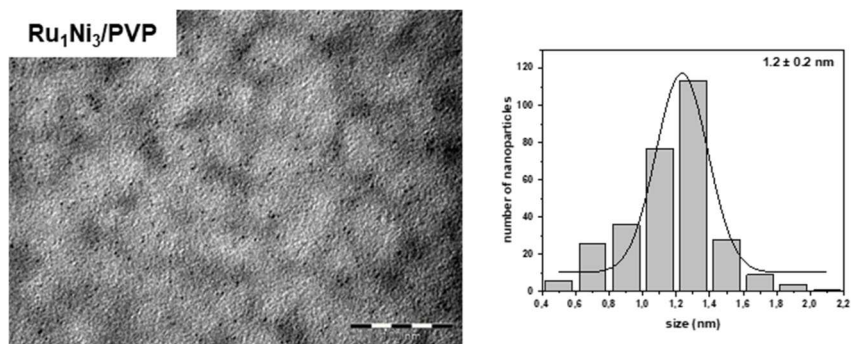


Figure S4. TEM image of Ru₁Ni₃/PVP (scale bar 100 nm) together with the respective size histogram.

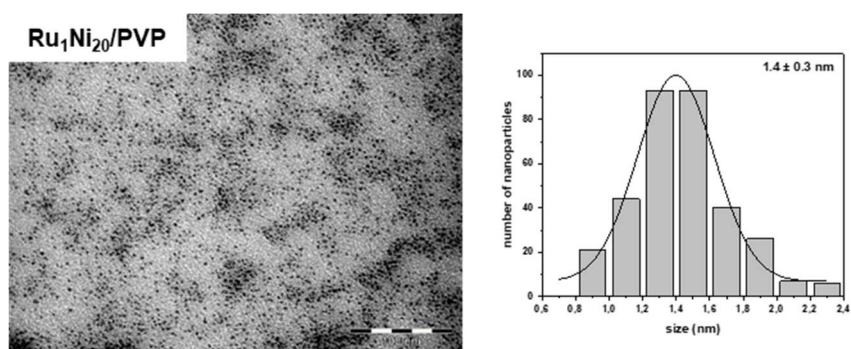


Figure S5. TEM image of Ru₁Ni₂₀/PVP (scale bar 100 nm) together with the respective size histogram.

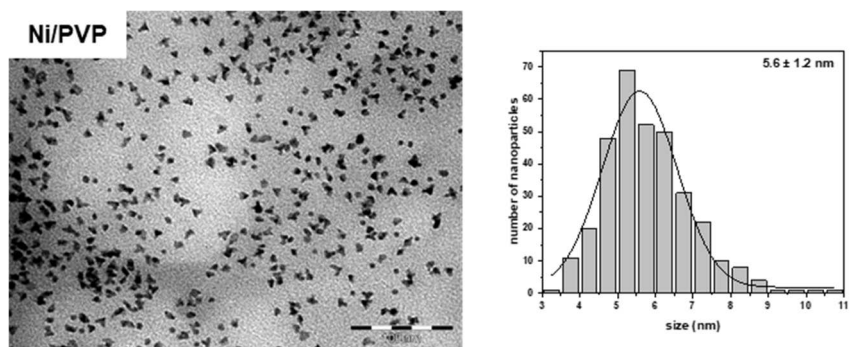


Figure S6. TEM image of Ni/PVP (scale bar 100 nm) together with the respective size histogram.

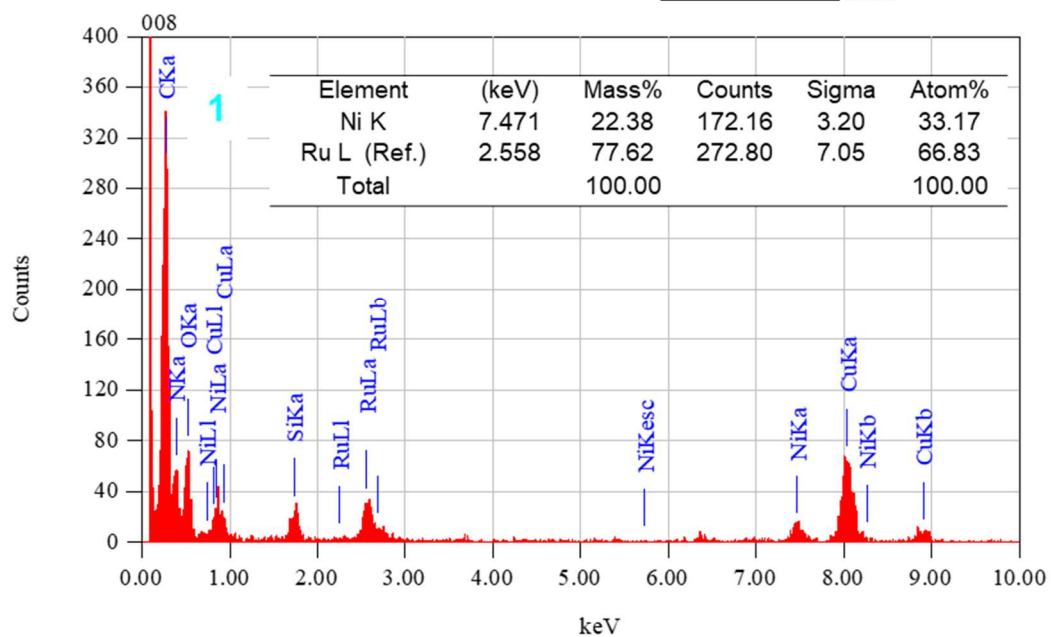
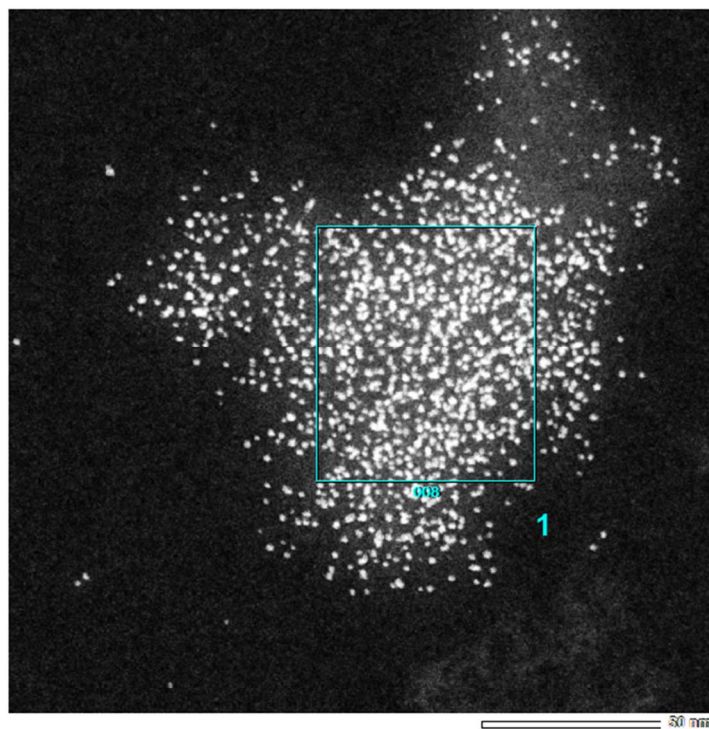


Figure S7. HAADF-STEM images of $\text{Ru}_1\text{Ni}_1/\text{PVP}$ synthesised at 85°C together with the EDX analysis of a set of nanoparticles.

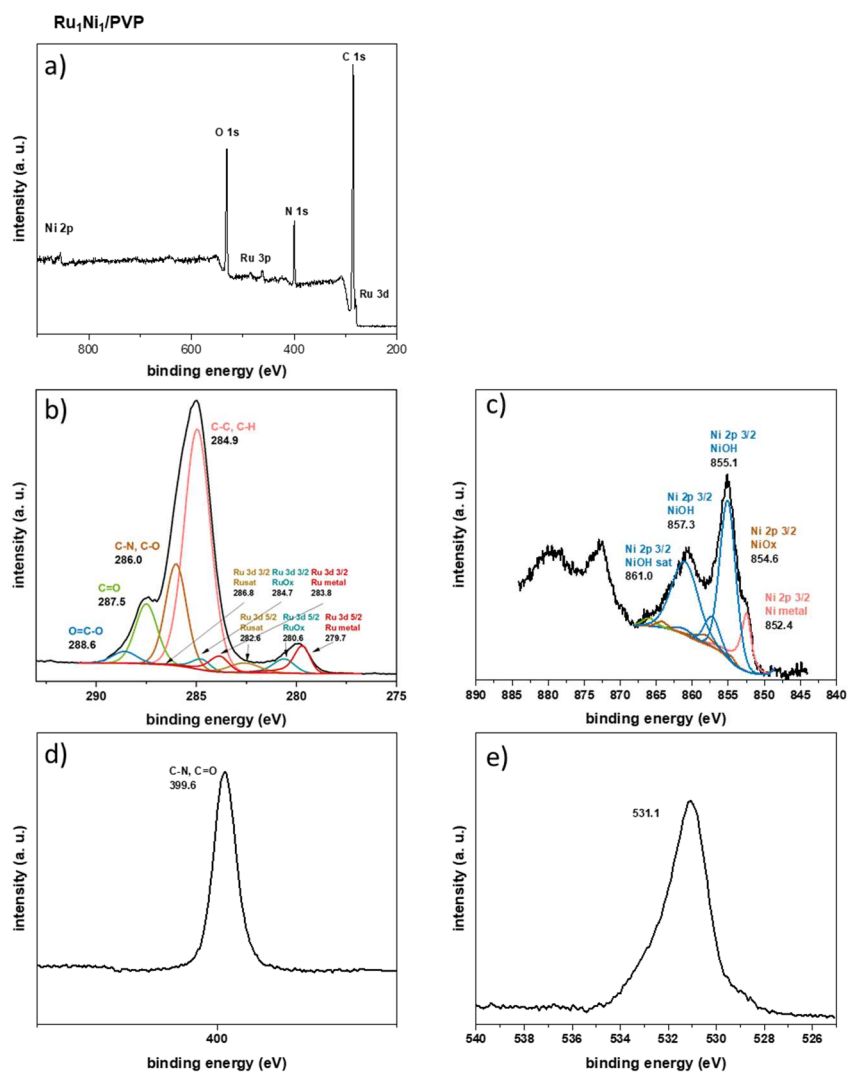


Figure S8. a) XPS survey spectrum of Ru₁Ni₁/PVP; and high-resolution scan spectra of b) C 1s and Ru 3d, c) Ni 2p, d) N 1s, and e) O 1s.

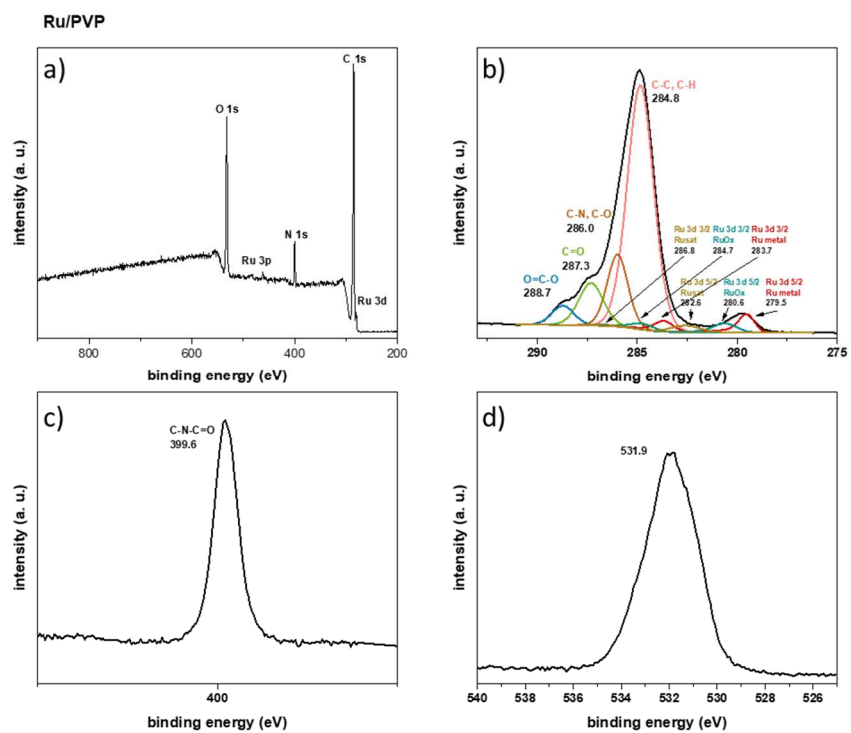


Figure S9. a) XPS survey spectrum of Ru/PVP; and high-resolution scan spectra of b) C 1s and Ru 3d, c) N 1s, and d) O 1s.

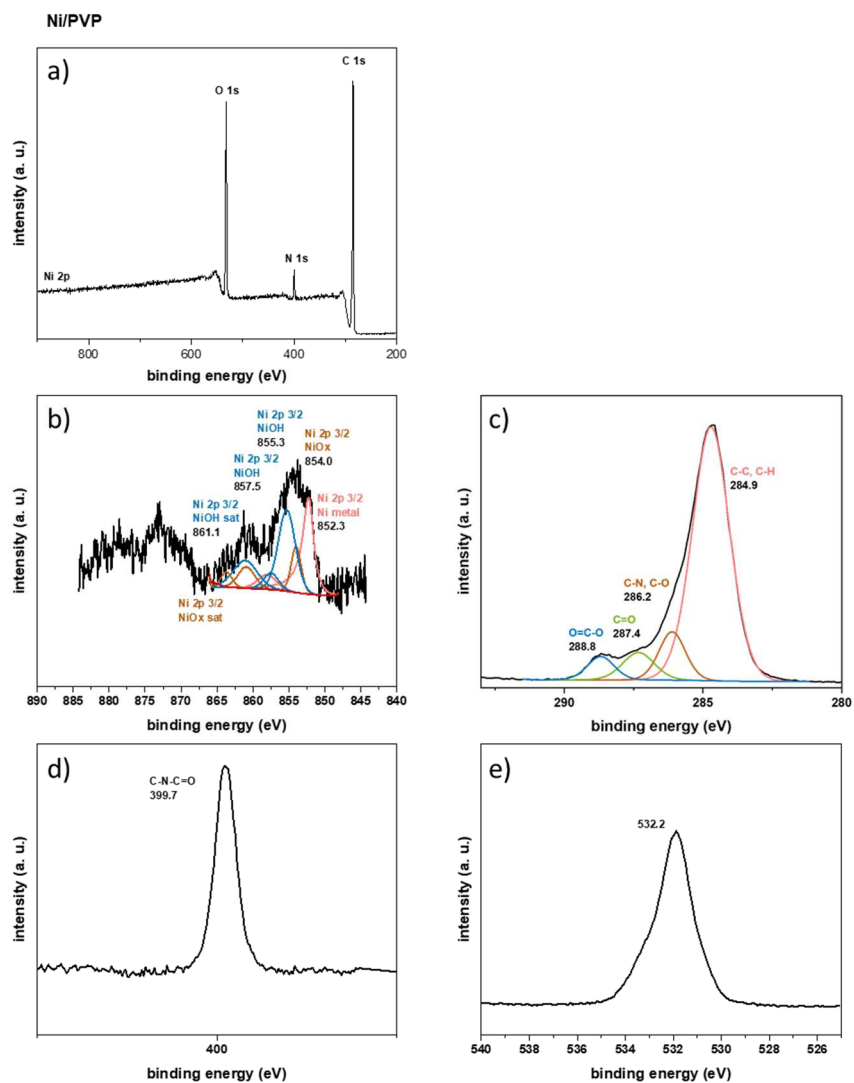


Figure S10. a) XPS survey spectrum of Ni/PVP; and high-resolution scan spectra of b) Ni 2p, d) C 1s, d) N 1s, and e) O 1s.

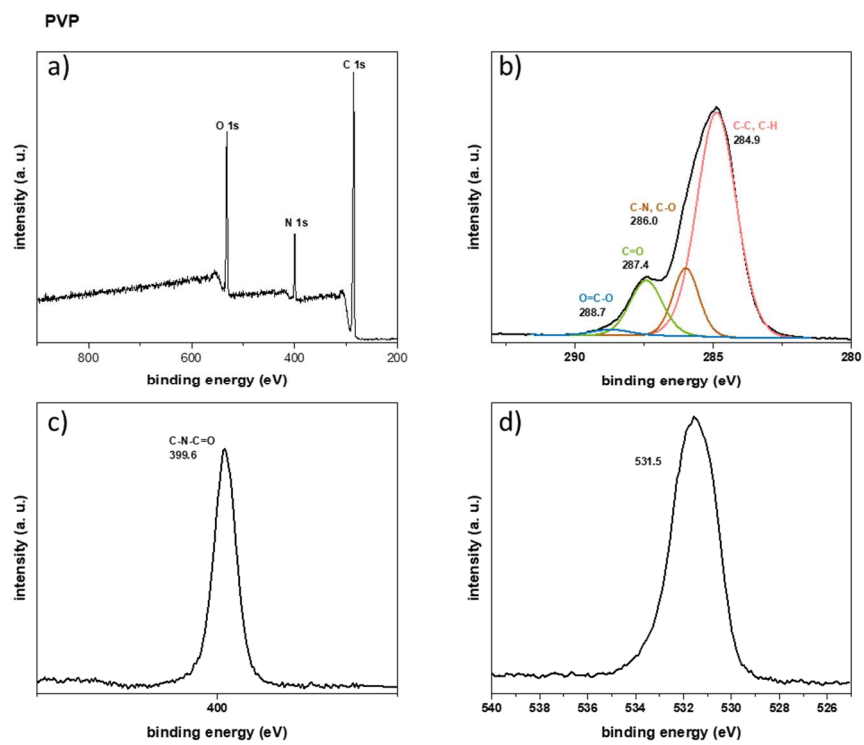


Figure S11. a) XPS survey spectrum of PVP; and high-resolution scan spectra of b) C 1s, c) N 1s, and d) O 1s.

Table S1. XPS Binding energies and atomic % of Ru/PVP, Ru₁Ni₁/PVP, Ni/PVP, and PVP.

	Ru/PVP		Ru ₁ Ni ₁ /PVP		Ni/PVP		PVP	
	Binding energy (eV)	Atomic %	Binding energy (eV)	Atomic %	Binding energy (eV)	Atomic %	Binding energy (eV)	Atomic %
Ru 3d 5/2 Ru metal	279.5	0.2	279.7	0.3	-	-	-	-
Ru 3d 5/2 RuOx	280.6	0.1	280.6	0.2	-	-	-	-
Ru 3d 5/2 Ru sat	282.6	0.1	282.6	0.2	-	-	-	-
Ru 3d 3/2 Ru metal	283.7	0.1	283.8	0.2	-	-	-	-
Ru 3d3/2 RuOx	284.7	0.1	284.7	0.1	-	-	-	-
C1s C-C, C-H	284.8	50.5	284.9	46.3	284.9	54.8	284.9	51.8
C1s C-N, C-O	286.0	11.8	286.0	15.9	286.2	9.1	286.0	10.4
Ru 3d3/2 Ru sat	286.8	0<0.1	286.8	<0.1	-	-	-	-
C 1s C=O	287.3	8.2	287.5	9.8	287.4	5.0	287.4	10.4
C 1s O=C-O	288.7	3.3	288.6	2.1	288.8	4.3	288.7	1.3
N 1s C-N-C=O	399.6	7.1	399.6	9.3	399.7	4.2	399.6	9.7
O 1s	531.9	18.5	531.1	14.8	532.2	22.5	531.5	16.4
Ni 2p 3/2 Ni metal	-	-	852.4	0.1	852.3	<0.1	-	-
Ni 2p 3/2 NiOx/Ni(OH)	-	-	around 855.1	0.8	around 855.0	<0.1	-	-

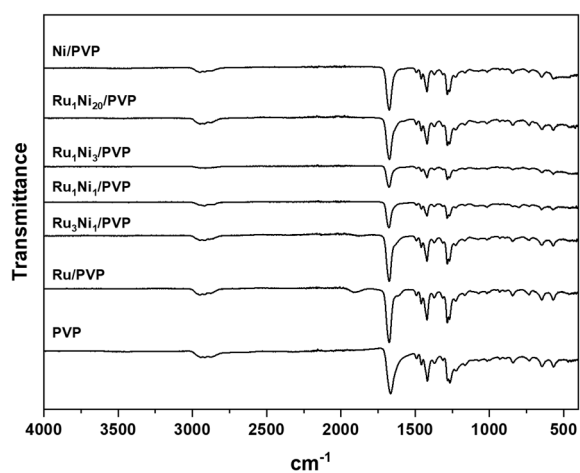


Figure S12. ATR-IR spectra of RuNi/PVP nanoparticles together with monometallic Ru and Ni nanoparticles, and PVP.

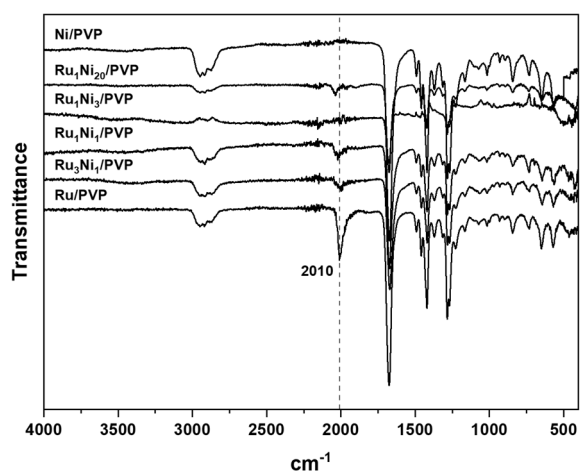


Figure S13. ATR-IR spectra of RuNi/PVP nanoparticles together with monometallic Ru and Ni nanoparticles after CO exposure.

Table S2. Estimation of Ni coverage on RuNi/PVP.

NP	NP composition (from ICP) ^a	Mean size (nm) ^b	Estimated total atoms on the NP ^c	Estimated atoms on the core ^c	Estimated atoms on the surface ^c	Estimated atoms surface (%) ^c	Estimated number of Ru atoms in a NP ^d	Estimated number of Ni atoms in a NP ^d	Estimated surface coverage of Ni (%) ^e
Ru/PVP	Ru/PVP	1.1 ± 0.2	51	11	40	77	51	0	0
Ru ₃ Ni ₁ /PVP	Ru _{2.7} Ni _{1.0} /PVP	1.5 ± 0.3	130	47	83	63	94	36	≈43
Ru ₁ Ni ₁ /PVP	Ru _{1.0} Ni _{1.0} /PVP	1.5 ± 0.3	130	47	83	63	66	64	≈77
Ru ₁ Ni ₃ /PVP	Ru _{1.0} Ni _{3.2} /PVP	1.2 ± 0.2	82	29	53	65	26	62	≈116
Ru ₁ Ni ₂₀ /PVP	Ru _{1.0} Ni _{20.0} /PVP	1.4 ± 0.3	131	55	76	58	6	125	>2 shell

^aICP analysis. ^bMean values of nanoparticle size determined from TEM images by considering at least 200 particles. ^cHigh Ru loaded NP (Ru/PVP, Ru₃Ni₁/PVP, and Ru₁Ni₁/PVP) were calculated as follows: the number of Ru atoms in *hcp* cell (N) is 6. The shell thickness is assumed as the half of the lattice constant, for Ru is 0.214 nm. The volume of Ru cell is 0.0817 nm³. R_{NP} represents the radius of NP. The volume of all Ru atoms on the shell of NP: $V_{shell} = V_{total} - V_{core} = 4/3\pi R_{NP}^3 - 4/3\pi (R_{NP} - R_{Ru})^3$, V_{total} meaning the volume of one Ru nanoparticle, V_{core} presenting the volume of NP excluded the one outer layer of atoms. The numbers of metal atoms on the shell N_{shell} = N * V_{shell} / 0.0817. The number of total Ru atoms N_{total} = N * V_{total} / 0.0817. The percentage of Ru atoms on the surface of NP = N_{shell} / N_{total} * 100%. High Ni loaded NP (Ru₁Ni₃/PVP and Ru₁Ni₂₀/PVP) were calculated as follows: the number of Ni atoms in *fcc* cell (N) is 4. The shell thickness is assumed as the half of the lattice constant, for Ni is 0.176 nm. The volume of Ni cell is 0.0438 nm³. R_{NP} represents the radius of NP. The volume of all Ru atoms on the shell of NP: $V_{shell} = V_{total} - V_{core} = 4/3\pi R_{NP}^3 - 4/3\pi (R_{NP} - R_{Ni})^3$, V_{total} meaning the volume of one Ni nanoparticle, V_{core} presenting the volume of NP excluded the one outer layer of atoms. The numbers of Ni atoms on the shell N_{shell} = N * V_{shell} / 0.0438. The number of total Ni atoms N_{total} = N * V_{total} / 0.0438. The percentage of metal atoms on the surface of NP = N_{shell} / N_{total} * 100%. ^dEstimated total atoms on the NP * metallic content (in mol). ^eEstimated number of Ni atoms in a NP / Estimated atoms on the surface * 100.

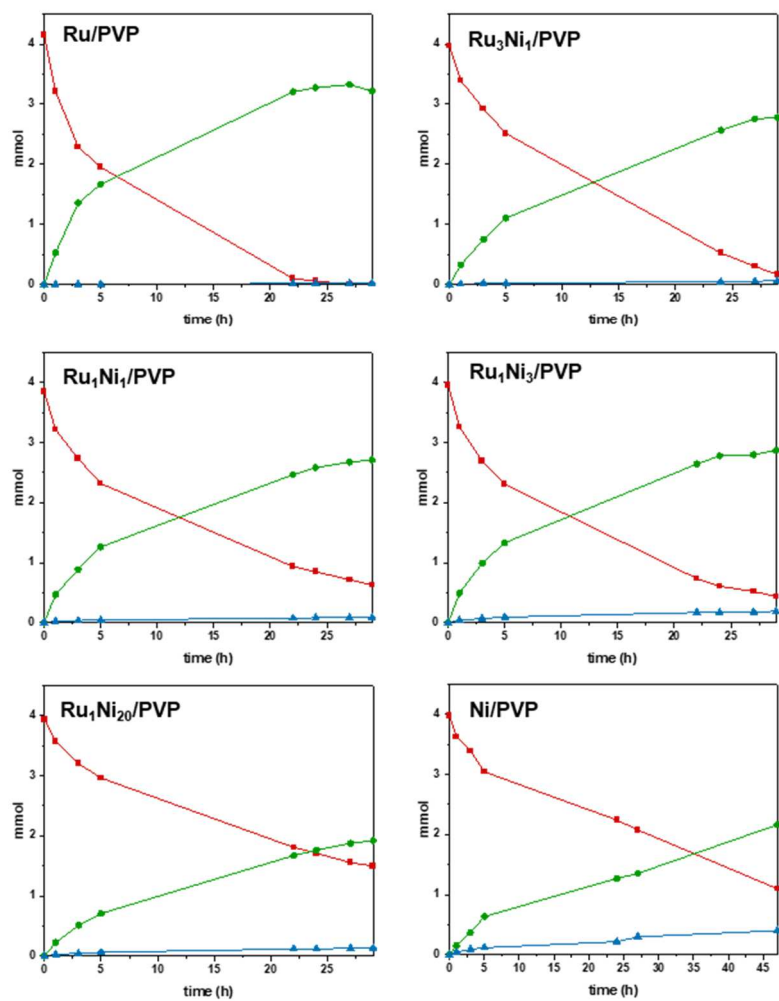


Figure S14. Time-concentration curves for the selective hydrogenation of furfural in THF using several catalysts (red square dots, furfural; green circle dots, 2-(hydroxymethyl)furan; blue triangle dots, tetrahydrofurfuryl alcohol).

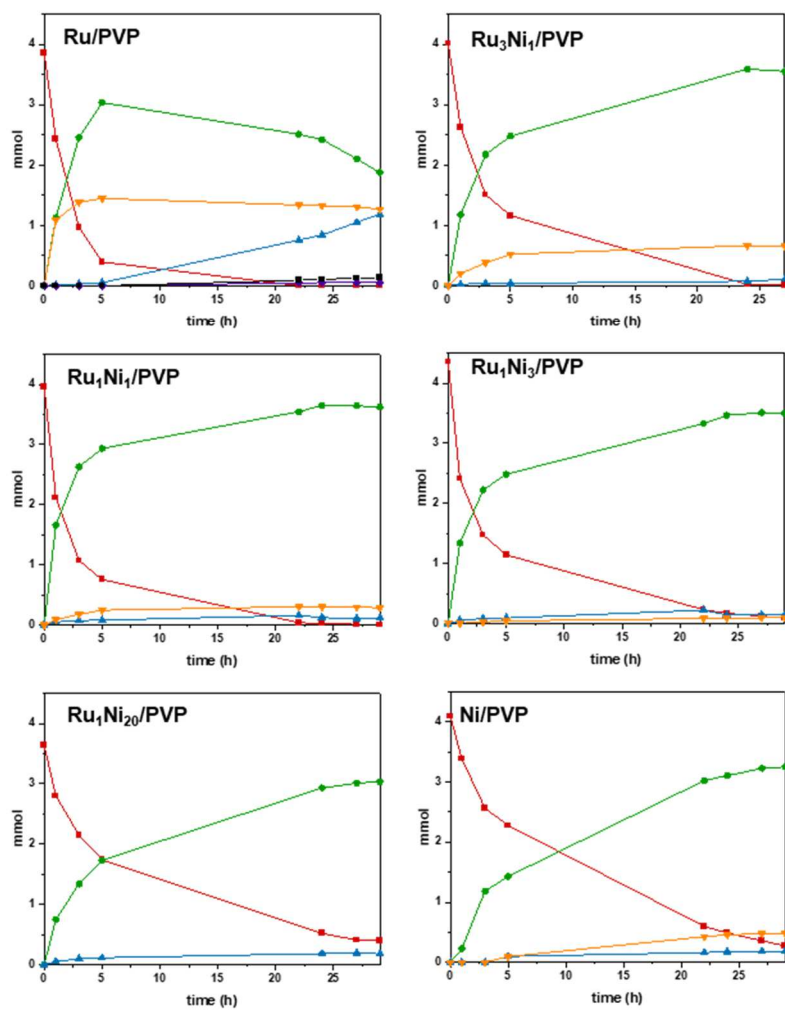


Figure S15. Time-concentration curves for the selective hydrogenation of furfural in 1-propanol using several catalysts (red square dots, furfural; green circle dots, 2-(hydroxymethyl)furan; blue triangle dots, tetrahydrofurfuryl alcohol; orange inverted triangle dots, acetal).

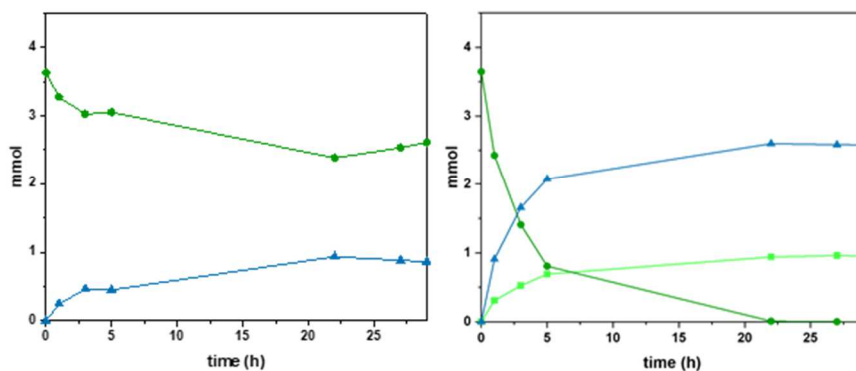


Figure S16. Time-concentration curves for the selective hydrogenation of 2-(hydroxymethyl)furan in THF (left) and in 1-propanol (right) using Ru/PVP as catalyst (green circle dots, 2-(hydroxymethyl)furan; blue triangle dots, tetrahydrofurfuryl alcohol; bright green square dots, 1, 2-pentanediol).

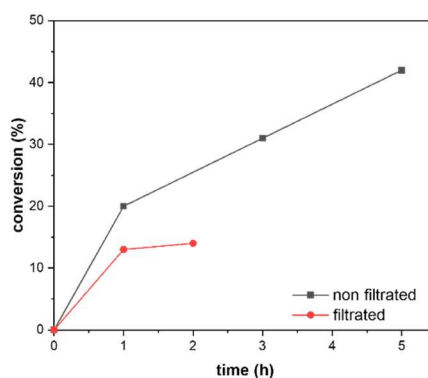


Figure S17. Hot filtration experiment. Time-conversion curves for the selective hydrogenation of furfural in THF using Ru₁Ni₁/PVP as catalyst, grey square dots, non-filtered reaction, red circle dots, filtered reaction.

Table S3. Mean size of metal nanoparticles before and after catalysis

NP	Mean size	Mean size	Mean size
	before catalysis (nm) ^a	after catalysis in THF (nm) ^a	after catalysis in 1-propanol (nm) ^a
Ru/PVP	1.0 ± 0.2	1.6 ± 0.3	1.5 ± 0.3
Ni/PVP	5.5 ± 1.2 ^b	4.4 ± 0.5 ^c	4.7 ± 1.6 ^c
Ru ₃ Ni ₁ /PVP	1.5 ± 0.3	1.4 ± 0.4	1.6 ± 0.5
Ru ₁ Ni ₁ /PVP	1.5 ± 0.3	1.5 ± 0.4	1.4 ± 0.4
Ru ₁ Ni ₃ /PVP	1.2 ± 0.2	1.3 ± 0.3	1.5 ± 0.6
Ru ₁ Ni ₂₀ /PVP	1.4 ± 0.3	1.6 ± 0.3	2.2 ± 0.8

^aMean values of nanoparticle size determined from TEM images by considering at least 200 particles. ^bTripodal shaped nanoparticles. ^cIrregularly shaped nanoparticles.

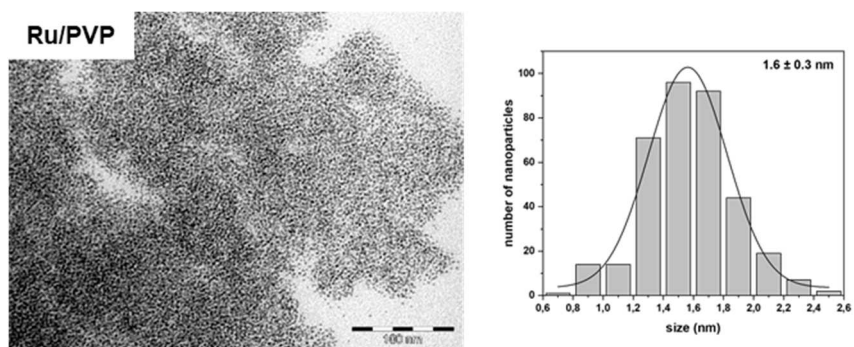


Figure S18. TEM image of Ru/PVP after catalysis in THF (scale bar 100 nm) together with the respective size histogram.

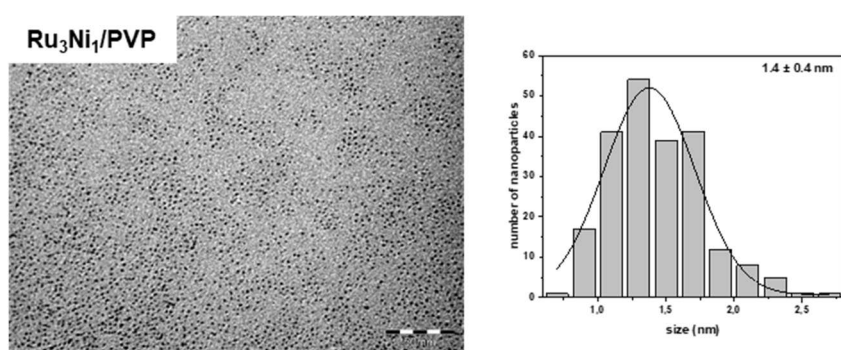


Figure S19. TEM image of Ru₃Ni₁/PVP after catalysis in THF (scale bar 50 nm) together with the respective size histogram.

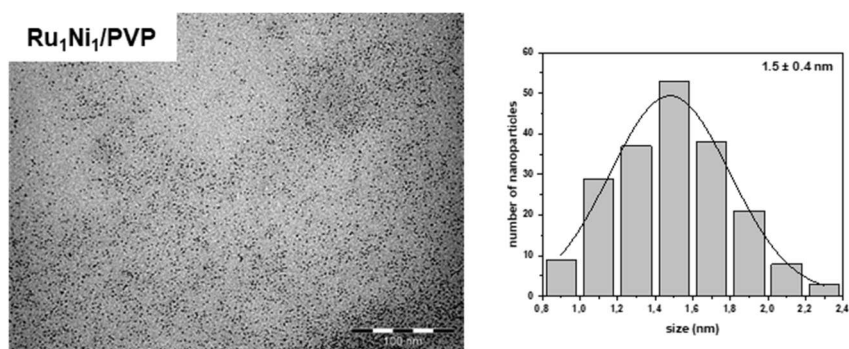


Figure S20. TEM image of Ru₁Ni₁/PVP after catalysis in THF (scale bar 100 nm) together with the respective size histogram.

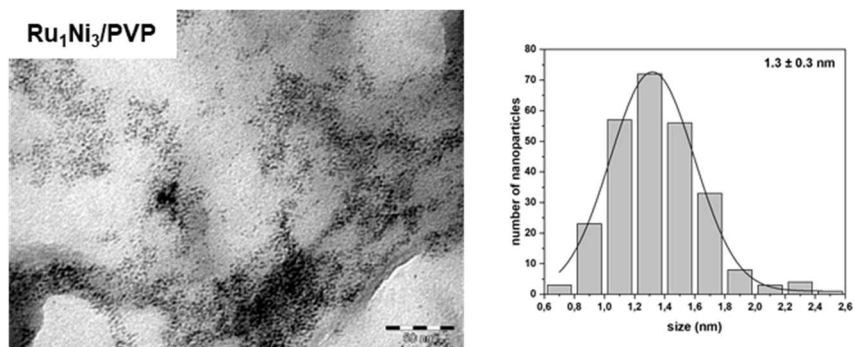


Figure S21. TEM image of Ru₁Ni₃/PVP after catalysis in THF (scale bar 50 nm) together with the respective size histogram.

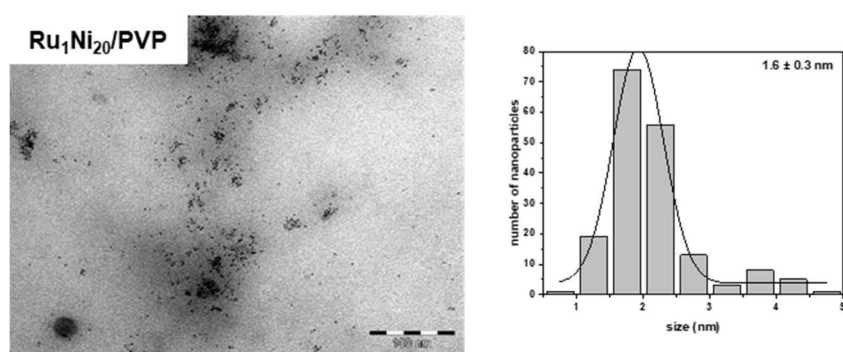


Figure S22. TEM image of Ru₁Ni₂₀/PVP after catalysis in THF (scale bar 100 nm) together with the respective size histogram.

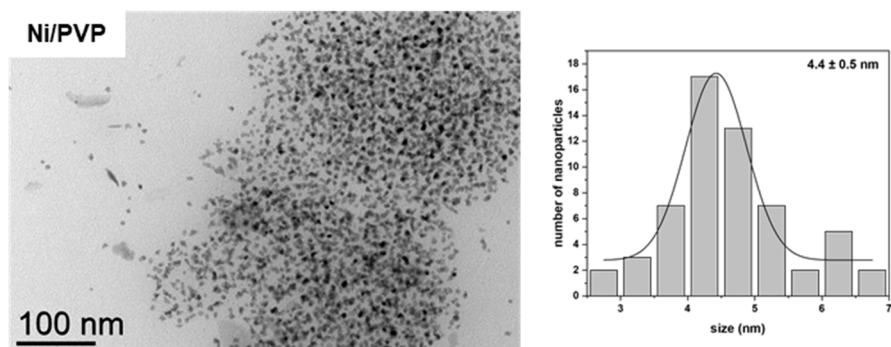


Figure S23. TEM image of Ni/PVP after catalysis in THF (scale bar 100 nm) together with the respective size histogram.

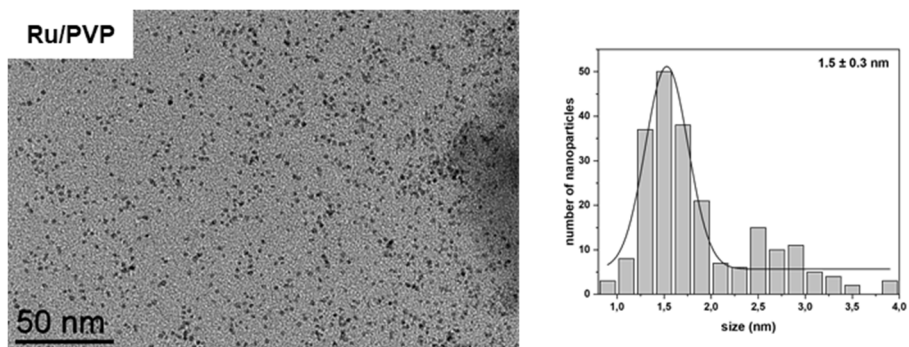


Figure S24. TEM image of Ru/PVP after catalysis in 1-PrOH (scale bar 100 nm) together with the respective size histogram.

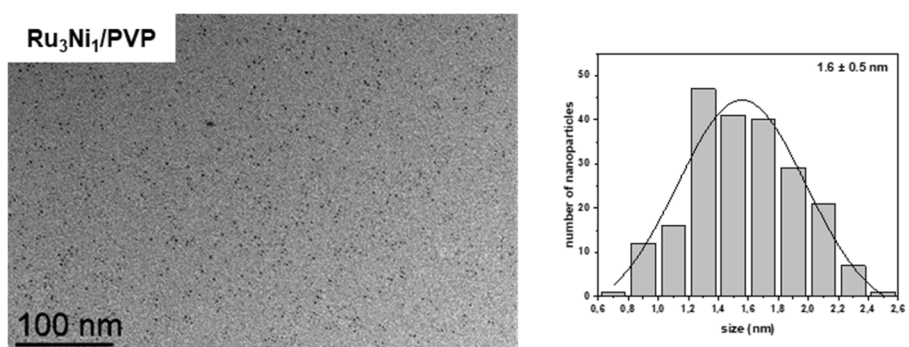


Figure S25. TEM image of Ru₃Ni₁/PVP after catalysis in 1-PrOH (scale bar 100 nm) together with the respective size histogram.

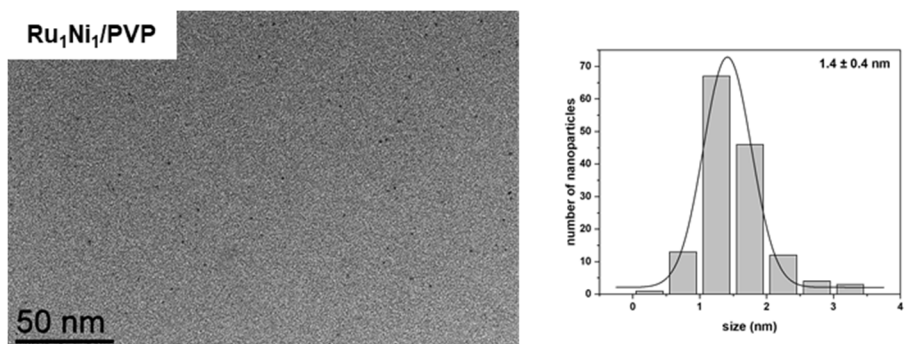


Figure S26. TEM image of Ru₁Ni₁/PVP after catalysis in 1-PrOH (scale bar 50 nm) together with the respective size histogram.

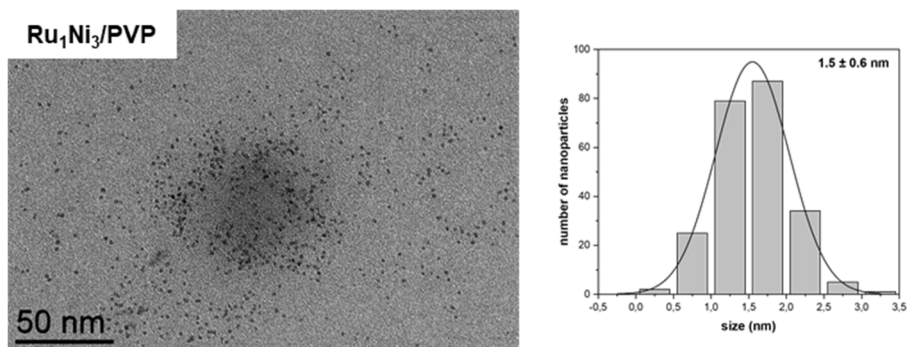


Figure S27. TEM image of Ru₁Ni₃/PVP after catalysis in 1-PrOH (scale bar 50 nm) together with the respective size histogram.

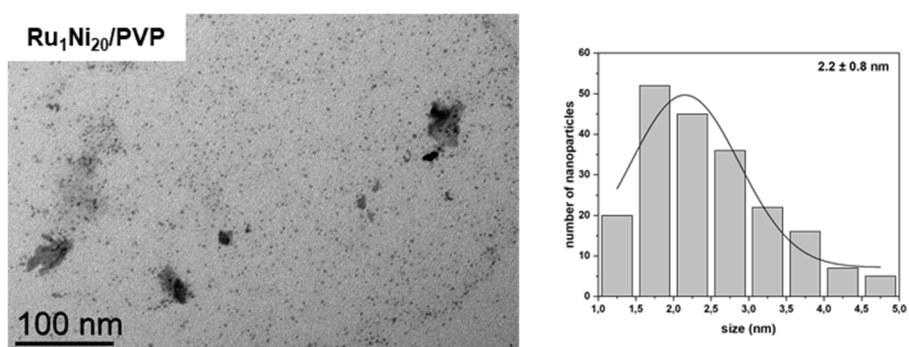


Figure S28. TEM image of Ru₁Ni₂₀/PVP after catalysis in 1-PrOH (scale bar 100 nm) together with the respective size histogram.

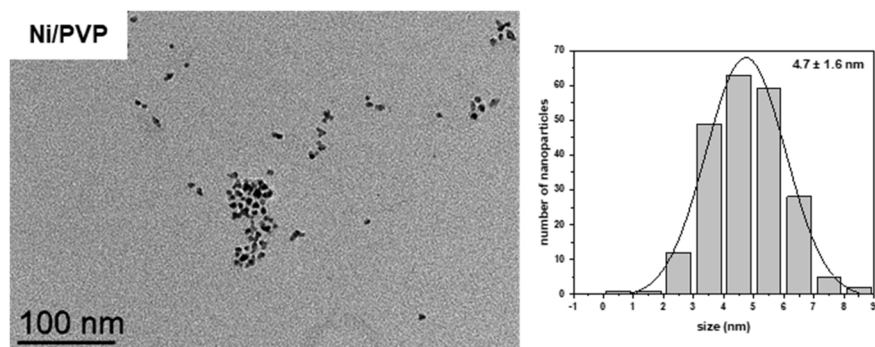


Figure S29. TEM image of Ni/PVP after catalysis in 1-PrOH (scale bar 100 nm) together with the respective size histogram.

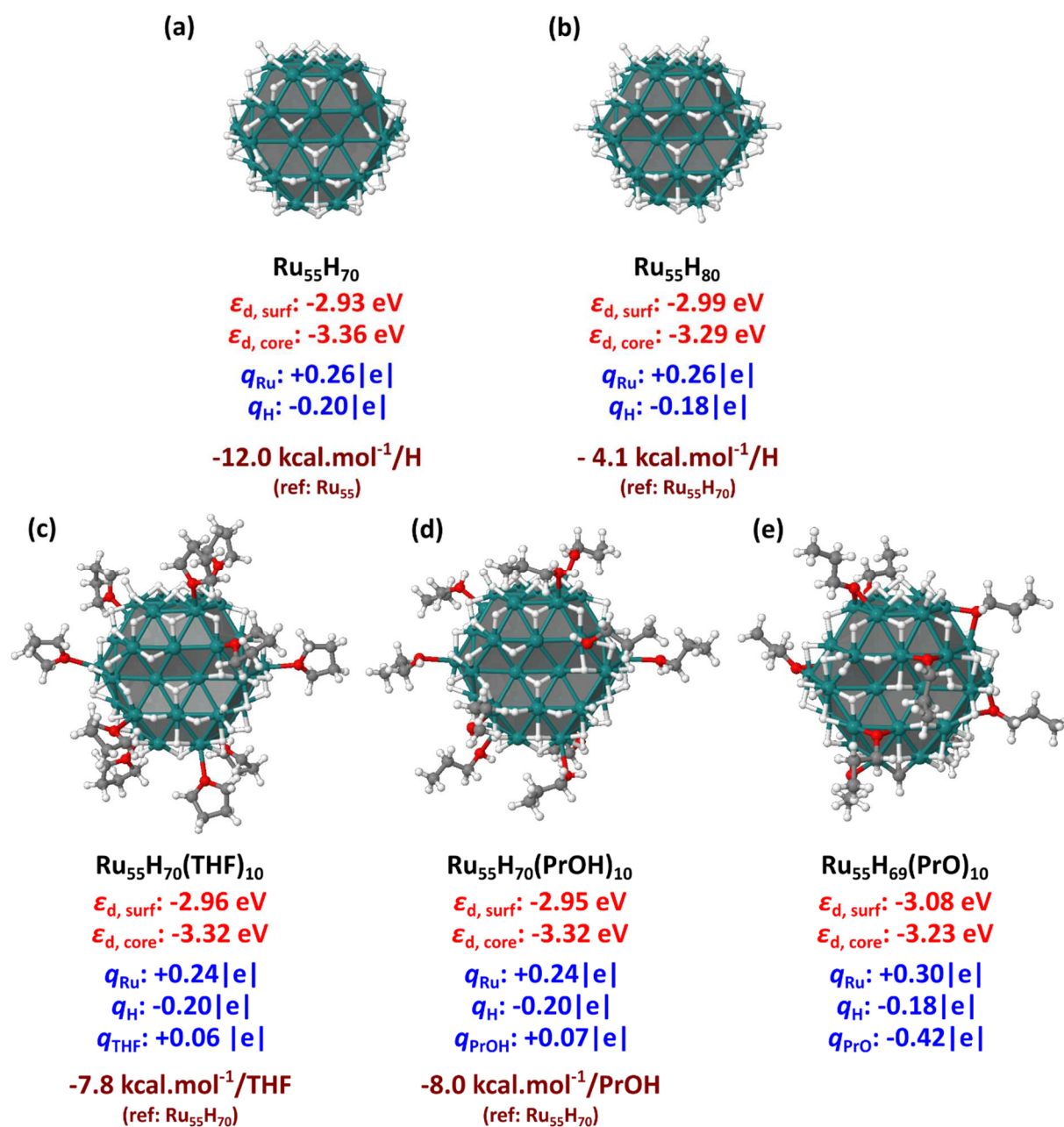
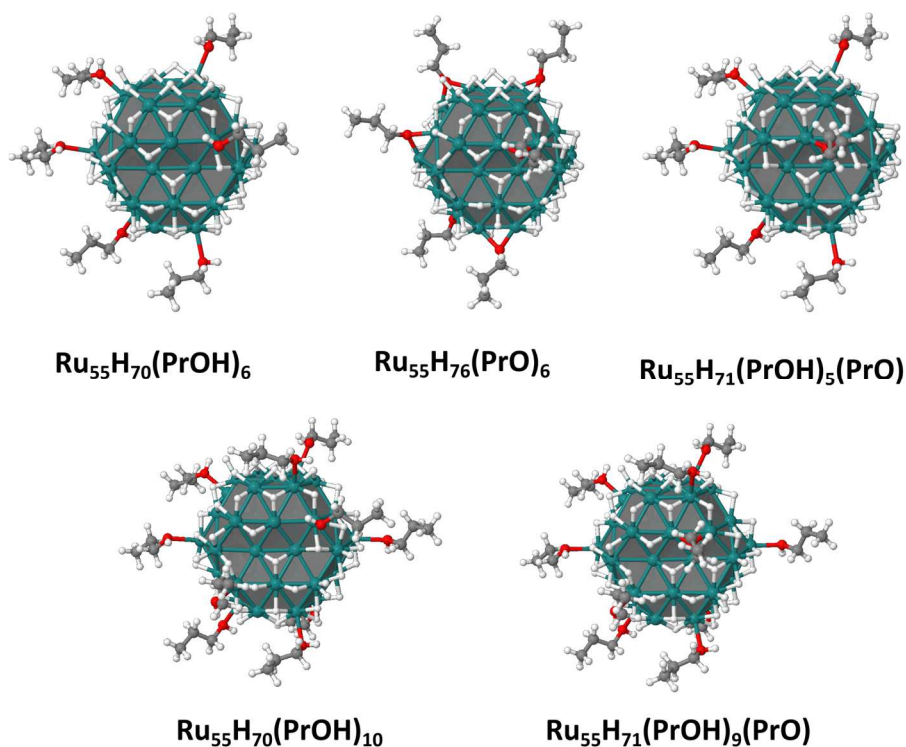


Figure S30. Comparison of adsorption energies per ligand, d-band center values of surface ($\epsilon_{d, surf}$) and core ($\epsilon_{d, core}$) Ru atoms, and average charges of hydrides (q_H) and metal atoms (q_{Ru}). Ru₅₅H₆₉(PrO)₁₀ was only considered to hypothetically assess the influence of ten propanolate ligands on the surface.



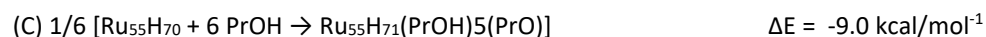
The adsorption of 6 PrOH is exothermic:



The dissociative adsorption of all six PrOH species is unfavorable:



However, in this case the dissociative adsorption of one PrOH among 6 is possible. Given the energies, it would be a well-balanced equilibrium on the surface: $\text{PrOH}^* \leftrightarrow (\text{PrO}^* + \text{H}^*)$



The adsorption of 10 PrOH on the surface is still exothermic:



In this case, the dissociative adsorption equilibrium of one PrOH among 10 is significantly in favor of the propanolate. The energy yields of reactions (C), (D), (F) and (G) suggest that the formation of PrO on the surface does not involve a thermodynamic malus.

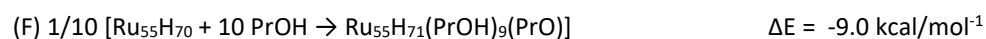


Figure S31. Dissociative or non-dissociative adsorption of 1-propanol on the $\text{Ru}_{55}\text{H}_{70}$ model.

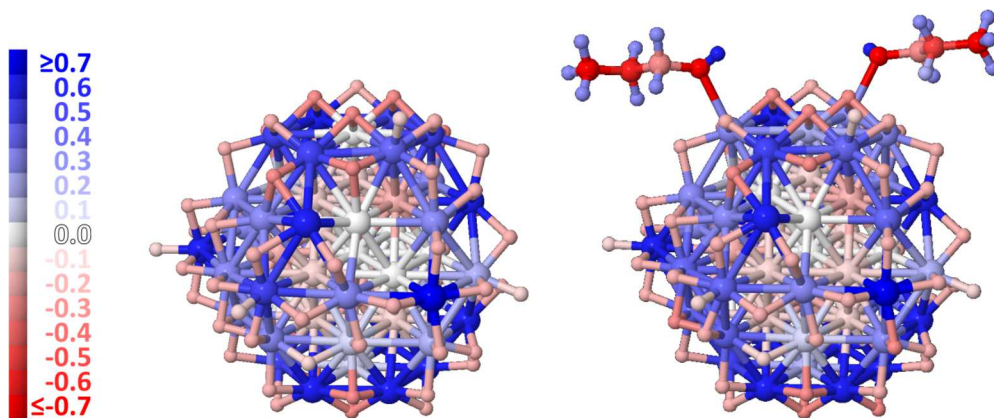


Figure S32. Atomic charges of the two model systems plotted as color maps (same models as in Figure 6, main text). Surface ruthenium atoms, in blue, are oxidized by all hydrides (average charges: $q_{\text{Hydride}} = -0.20$ in both models, $q_{\text{H(OH)}} = +0.54$).

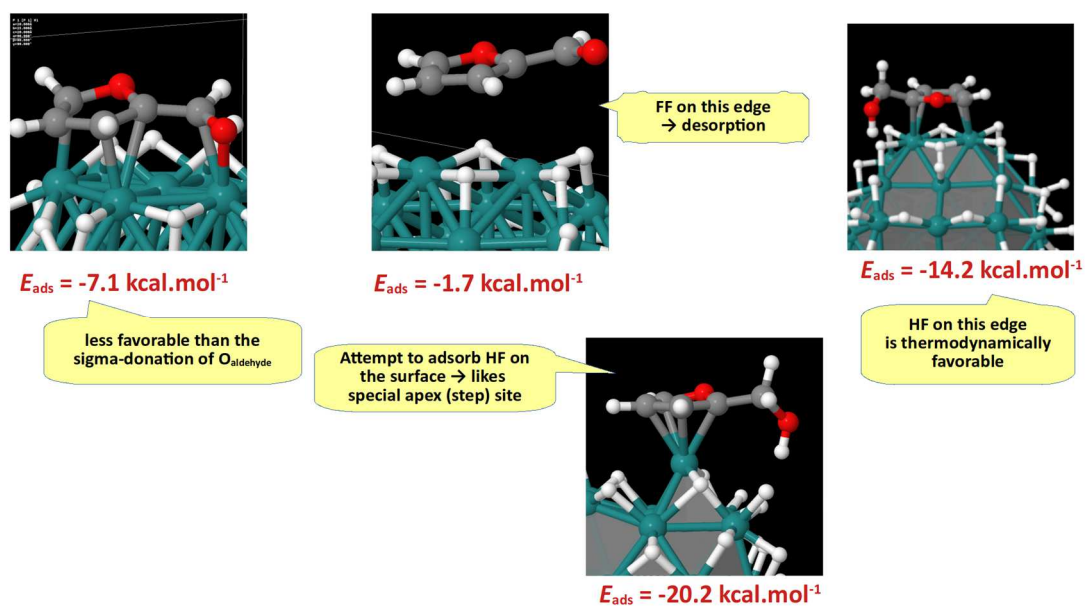


Figure S33. Possible π adsorption of 2-(hydroxymethyl)furan (HF), or furfural (FF), preliminary to the hydrogenation step of the furanyl cycle. Energies are given in kcal.mol^{-1} .

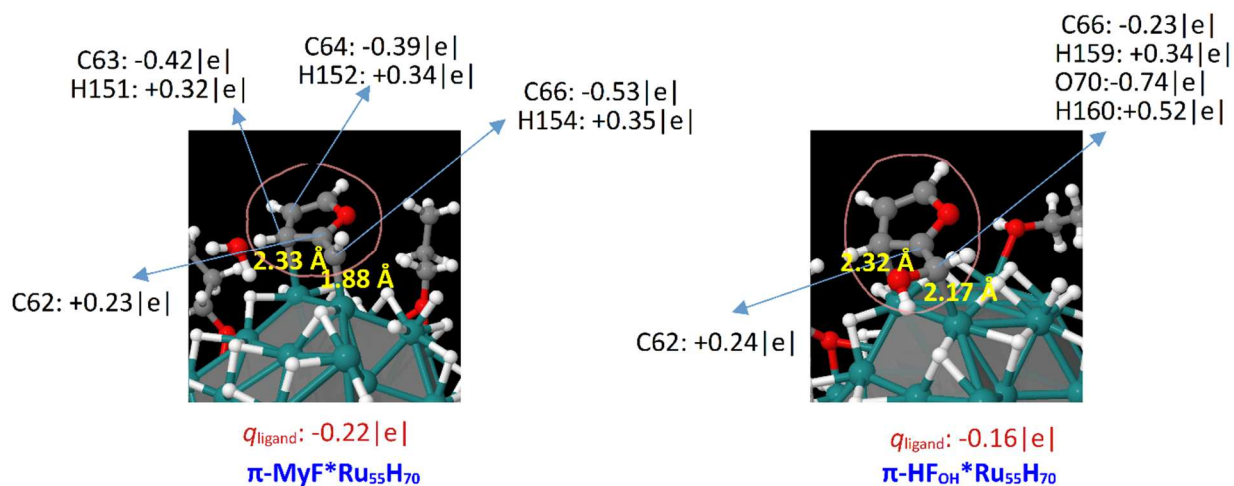


Figure S34. Comparison between $\pi\text{-MyF}^*\text{Ru}_{55}\text{H}_{70}$ and $\pi\text{-HF}_{\text{OH}}^*\text{Ru}_{55}\text{H}_{70}$ of selected geometry parameters and charges. $\pi\text{-MyF}^*\text{Ru}_{55}\text{H}_{70}$ is a dimetallacycle intermediate found on the acetal formation pathway. A vibrational analysis confirmed that it is a minimum on the potential energy surface. See also Figure 11, main text. The short Ru-C_{methyne}(sp²) bond length in this intermediate and the negative charge on the methyne fragment both suggest a kind of Ru=C double bond.